Geomorphology 304 (2018) 99–112

Contents lists available at ScienceDirect

Geomorphology

journal homepage: www.elsevier.com/locate/geomorph

The influence of tributary flow density differences on the hydrodynamic behavior of a confluent meander bend and implications for flow mixing

Herrero Horacio S. [a], Díaz Lozada José M. [a,b,*], García Carlos M. [a,b], Szupiany Ricardo N. [b,c], Best Jim [d], Pagot Mariana [e]

[a] Institute for Advanced Studies for Engineering and Technology (IDIT CONICET/UNC) and CETA – FCEFyN (UNC), Av. Velez Sarsfield 1611, Ciudad Universitaria, Córdoba, Argentina
[b] National Scientific and Technical Research Council (CONICET), Argentina
[c] Facultad de Ingeniería y Ciencias Hídricas, Centro Internacional de Estudios de Grandes Ríos (CIEGRI), National University of Littoral, Santa Fe, Argentina
[d] Departments of Geology, Geography and GIS, Mechanical Science and Engineering and Ven Te Chow Hydrosystems Laboratory, University of Illinois at Urbana-Champaign, Champaign, IL, USA
[e] Laboratorio de Hidráulica, FCEFyN, National University of Córdoba, Córdoba, Argentina

ARTICLE INFO

Article history:
Received 29 June 2017
Received in revised form 14 December 2017
Accepted 18 December 2017
Available online 27 December 2017

Keywords:
River confluence
Hydrodynamics
Mixing
Experimental work

ABSTRACT

The goal of this study is to evaluate the influence of tributary flow density differences on hydrodynamics and mixing at a confluent meander bend. A detailed field characterization is performed using an Acoustic Doppler Current Profiler (ADCP) for quantification of the 3D flow field, flow discharge and bathymetry, as well as CTD measurements (conductivity, temperature, depth) to characterize the patterns of mixing. Satellite images of the confluence taken at complementary times to the field surveys were analyzed to evaluate the confluence hydrodynamics at different flow conditions.

The results illustrate the differences in hydrodynamics and mixing length in relation to confluences with equal density tributaries. At low-density differences, and higher discharge ratio (Q_r) between the two rivers, the flow is similar to equi-density confluent meander bends. In contrast, at high-density differences (low Q_r), the tributary flow is confined to near the confluence but the density difference causes the flow to move across channel. In this case, the density difference causes the lateral spread of the tributary flow to be greater than at a greater Q_r when the density difference is less. These results illustrate the potential importance of density differences between tributaries in determining the rate and spatial extent of mixing and sediment dispersal at confluent meander bends.

1. Introduction

The characterization of flow at channel confluences is an aspect of fluvial research that has generated great interest over the last 30 yr. (see review of Best and Rhoads, 2008), with much focus on the characterization of the junction hydrodynamics and mixing patterns between the two convergent flows. Previous work includes the study of confluences in laboratories (Mosley, 1976; Best, 1986, 1987, 1988; Best and Roy, 1991; Biron et al., 1996a, 1996b; McLelland et al., 1996; Herrero et al., 2016), in small rivers (Best and Reid, 1984; Roy et al., 1988; Roy and Bergeron, 1990; Ashmore et al., 1992; Bristow et al., 1993; Biron et al., 1993a, 1993b; Kenworthy and Rhoads, 1995; Rhoads and Kenworthy, 1995; McLelland et al., 1996; Rhoads, 1996; De Serres et al., 1999; Rhoads and Sukhodolov, 2001, 2004; Boyer et al., 2006; Rhoads et al., 2009; Riley and Rhoads, 2012; Ramón et al., 2013, 2014; Lewis and Rhoads, 2015) and in large channels (Best and Ashworth, 1997; Parsons et al., 2007; Szupiany et al., 2007; Lane et al., 2008; Parsons et al., 2008; Laraque et al., 2009; Szupiany et al., 2009; Trevethan et al., 2015).

The knowledge gained from these studies has allowed development of several models of flow dynamics for different types of confluences. Mosley (1976) and Best (1986) developed conceptual models of flow structure for symmetrical planform confluences, with Best (1987) outlining a model for asymmetrical planform junctions that has been widely adopted and recognizes five hydrodynamic regions: (a) flow stagnation; (b) flow deflection; (c) flow separation; (d) flow acceleration; and (e) flow recovery (Best, 1986, 1987). The characteristics of these zones are dependent on the confluence geometry, the angle between the converging flows, the momentum ratio and bed morphology. Sukhodolov and Rhoads (2001) proposed a hydrodynamic characterization of flow in confluences through an analogy with flow around an obstacle, which has recently been validated through laboratory tests by Herrero et al. (2016). With respect to confluent meander bends in sinuous rivers, this type of junction has been documented in several fluvial systems (Callaway, 1902; Davis, 1903; Flint, 1980; Hills, 1983; Abrahams, 1984a, 1984b), but the hydrodynamics have not been studied extensively. Due to advances in measurement techniques, confluences where one of the tributaries converges with the other on the outside a

* Corresponding author at: Centro de Estudios y Tecnología del Agua (CETA), National University of Córdoba, Córdoba, Argentina.
E-mail address: jmdiazlozada@unc.edu.ar (J.M. Díaz Lozada).

https://doi.org/10.1016/j.geomorph.2017.12.025
0169-555X/

bend have been characterized in more detail recently (Roberts, 2004; Riley and Rhoads, 2012; Riley et al., 2014). One of the first studies of confluent meander bends was that of Roberts (2004), who studied the 3D flow structure of a 90° confluent bend using numerical modeling and laboratory experiments, and developed a conceptual model for this type of junction (Fig. 1). Later, Riley and Rhoads (2012) characterized, by field measurements, the hydrodynamics of the confluent meander bend between the Little Wabash River and Big Muddy Creek, Illinois, USA, and compared these results with the conceptual model of Roberts (2004). Subsequently, Riley et al. (2014) analyzed the influence of the angle between confluent flows on the hydrodynamics and morphology. However, despite this recent literature concerning confluent meander bends in laboratory experiments and rivers, most of these studies have only focused on river confluences with equal density converging flows.

Fischer (1969) developed, by laboratory experimentation, an equation to compute the required length to achieve complete mixing downstream of channel junctions, with a maximum deviation of 5%. Fischer et al. (1979) adapted this relationship to a confluent bend with equal density tributaries allowing a good approximation for the mixing length, but its implementation presents issues in natural rivers (Rutherford, 1994) and has significant shortcomings with different density tributaries. Yotsukura and Sayre (1976) reported another expression to estimate the mixing length, but like Fischer's equation, this expression has a high uncertainty.

Past research, which has characterized confluences with different density tributaries, has indicated that the hydrodynamics of the confluence are affected by many factors, including: (a) suspended sediment concentration, (b) temperature, (c) dissolved solids concentration (d) momentum ratio between the two channels and (e) depth differential between the channels. The difference in densities may affect flow velocities and mixing processes (Weigold and Baborowski, 2009). Laraque et al. (2009) and Ramón et al. (2013) suggest that buoyancy may influence mixing at river confluences when density contrasts between tributary flows are relatively small. Lane et al. (2008) analyzed the hydrodynamics of the confluence of the Paraguay and Parana rivers, Argentina, where the Rio Paraguay has a higher density due its greater suspended sediment concentration. Lane et al. (2008) indicate that the rate of mixing between the two tributary flows depends on the momentum ratio, with larger tributary inputs producing higher penetration of the denser tributary under the less dense tributary, and creating a greater velocity differential at the junction, that promotes a greater rate of mixing. Lyubimova et al. (2014) analyzed, using numerical simulations and field measurements, the hydrodynamics of a confluence of different density tributaries, where the converging flows had different hydrochemical characteristics. Lewis and Rhoads (2015) examined the influence of the momentum flux ratio, the scale of the flow and the density differences between incoming flows, on thermal mixing at a small stream confluence. They concluded that where the incoming flows have a relatively high-density contrast, then buoyancy may influence the pattern of mixing, but that more work is needed on this topic. Although the influence of density differences between two confluent flows has been shown to be important (Maurice-Bourgoin et al., 2003; Moreira-Turcq et al., 2003; Laraque et al., 2009; Bouchez et al., 2010; Ramón et al., 2013, 2014; Lewis and Rhoads, 2015; Park and Latrubesse, 2015; Trevethan et al., 2015), the detailed mixing patterns and processes and underlying flow physics that may be operative in such conditions have not been fully documented. Previous studies of river confluences have thus not addressed the hydrodynamics of confluent meander bends where the tributaries possess different densities. Therefore, the main goal of the present study is to evaluate the influence of tributary density differences on the hydrodynamic behavior and mixing patterns at a river bend confluence.

2. Location of the field site

This paper details a study of the confluence of the Tercero (T) and Saladillo (S) rivers that is located in the Carcarañá River basin, southeast Córdoba Province, Argentina (32°54′55″S; 62° 19′29″W; Fig. 2). The drainage area of the basin upstream of the confluence (of both tributaries) is 50,900 km^2 (9700 km^2 in the Tercero River basin and 41,200 km^2 in the Saladillo River basin). The confluence studied herein is located on a meander bend with a radius of 65 m, where the Tercero River has an annual mean discharge of 27 m^3 s^{-1}, a mean depth of 0.93 m, and an average width of 40 m, and the Saladillo River has an

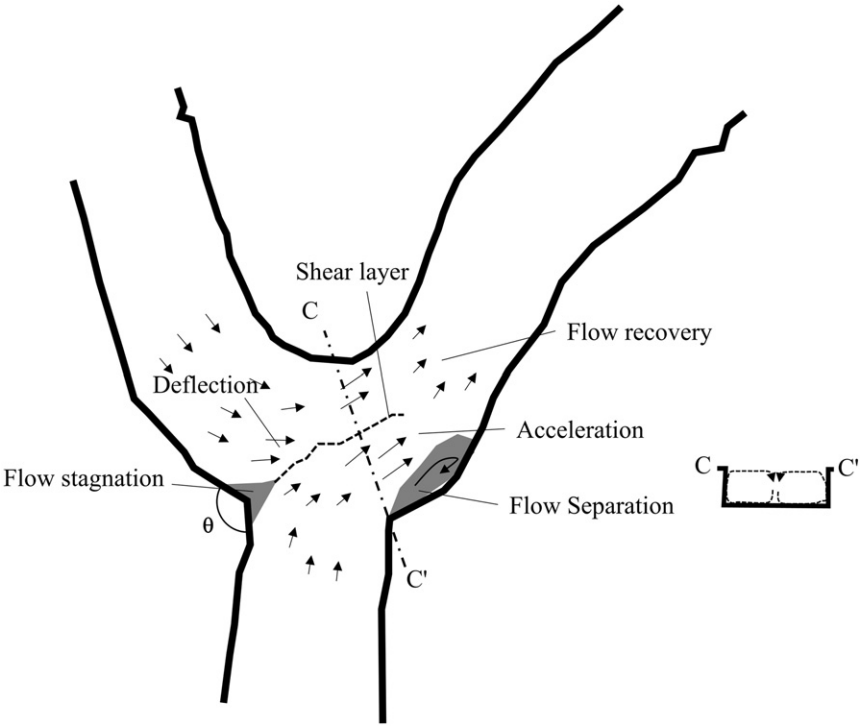

Fig. 1. Conceptual model of flow structure at a meander bend confluence (after Roberts, 2004).

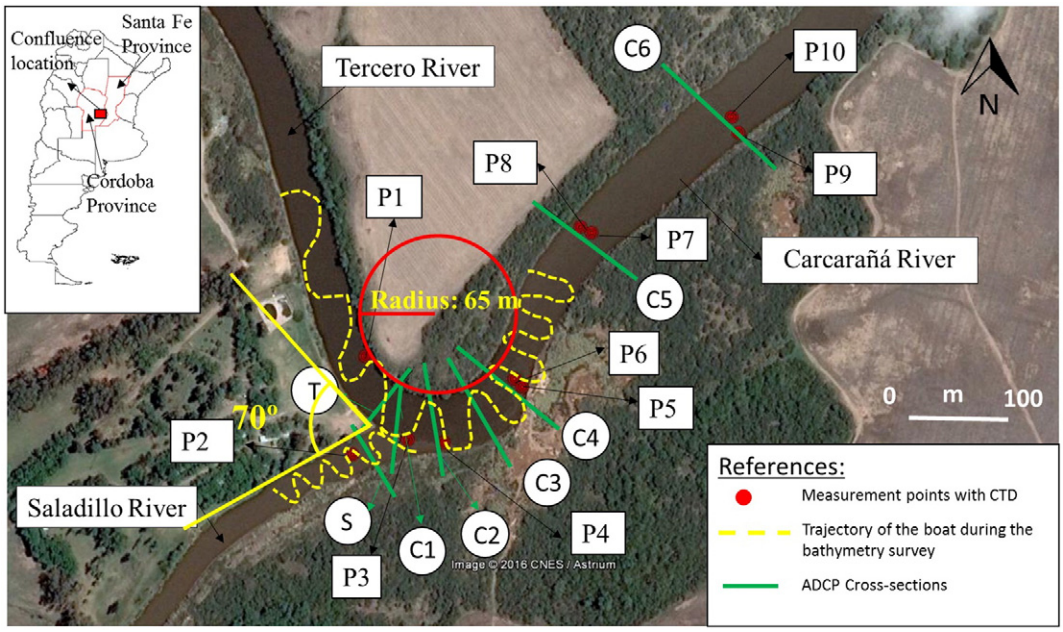

Fig. 2. The confluence between the Tercero and Saladillo rivers. The satellite image was taken on 10/14/2013. The figure shows the trajectory of the boat during the bathymetric survey, CTD measurement points and location of cross sections where flow discharge and hydraulic parameters were measured using ADCP. T = Tercero; S = Saladillo; C = Carcarañá.

annual mean discharge of 15 $m^3 s^{-1}$, a mean depth of 1.3 m, and an average width of 30 m. The channel gradients of both tributaries are of the order of 0.02%. The Saladillo River joins the Tercero River at an angle of 70° at the outer bank of the bend in the region of maximum curvature.

In the confluence studied herein, is not possible to define a dominant tributary because the discharge of the tributaries depends on the hydrometeorological events in the basin and the regulation of the reservoirs in the Tercero River, thus resulting in the Tercero River sometimes forming the main tributary or vice-versa (Díaz-Lozada et al., 2015). In this study, the Tercero River is defined as main stream and the Saladillo River as the tributary. Hydropeaking occurs in the Tercero River basin and produces changes in the flow discharge from the dams, but the last reservoir maintains a uniform streamflow in the river. Statistically, once a year the water level is above the level of the weir of the dams and the flow peak arrives at the confluence around seven days later. Previous observations of the confluence have also shown different hydrodynamic and mixing patterns dependent on the discharge of each tributary (Herrero, 2014). When the discharge of the Saladillo River is high, the confluence presents a behavior similar to that reported by Riley and Rhoads (2012), with mixing lengths greater than those generated when the discharge of the Saladillo River is low. When the Saladillo River flow discharge is low, it possesses a higher density than the Tercero River due to dissolved minerals, which produces complex hydrodynamic patterns and a mixing length that is shorter than at high Saladillo River discharges (Fig. 2).

The Tercero River watershed contains six reservoirs with a total reservoir capacity of 1000 Hm^3 that have a strong influence on the flow discharge of the river. The Saladillo River is the name of lower course of the Cuarto River (also named Chocancharava River), and although the basin does not contain any reservoirs, the river has been affected by changes in land use, drainage of wetlands and construction of channels, which produce an important seasonal variation in discharge (Díaz-Lozada et al., 2015). The Saladillo River receives underground water in the "Saladillo Wetlands" with high concentrations of chlorides, sulfates, arsenic and magnesium, which produces a higher salinity, and thus density, in the Saladillo River than the Tercero River at low and medium discharges. The evolution of water conductivity with flow discharge of the Tercero and Saladillo rivers at the confluence (Fig. 3) shows that the Saladillo River presents, in many cases, a higher conductivity than the Tercero River, which thus results in the Saladillo River possessing a higher density than the Tercero River. Temperature differences are not important at the junction (temperature differences < 10%).

3. Methods

The field measurements were conducted on August 13, 2013, when flows in the Tercero and Saladillo rivers were 19.9 $m^3 s^{-1}$ and 10.5 $m^3 s^{-1}$ respectively. To quantify discharge in each tributary, as well as characterize the flow at different measurement sections, a YSI/SonTek RiverSurveyor S5® 3 MHz ADCP with four beam Janus configuration was used. The main features of the SonTek RiverSurveyor S5 (Sontek, 2013) are: (a) discharge measurement profiling range (distance) from 0.3 to 15 m; (b) the cell size is selected automatically from 0.02 to 0.5 m according to the water velocity and depth; in this study cell sizes of 0.02 m and 0.10 m were selected automatically by the instrument; and (c) five transducers - four 3.0 MHz beams at a 25° slant angle for velocity and depth measurements and one 1.0 MHz vertical beam for depth measurement.

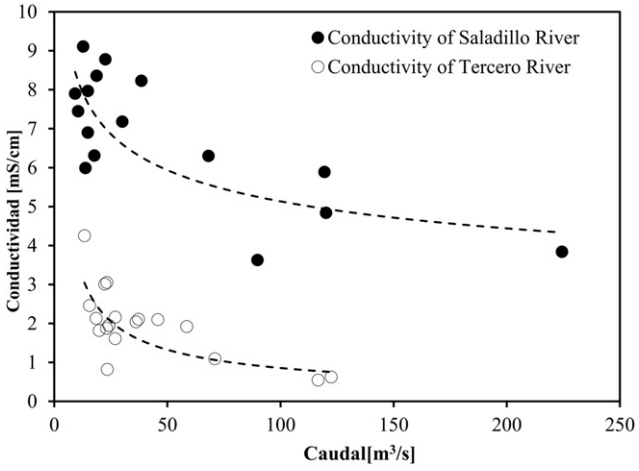

Fig. 3. Conductivity plotted against discharge for the Tercero and Saladillo rivers (from Díaz-Lozada, 2014 and updated with data to November 2016).

Eight cross sections were measured within the confluence area (S, T and C sections in Fig. 2). Each cross section in the Carcarañá River was made with one transect. Four transects (>12 min of measurement) were made in each cross section of each tributary to obtain adequate discharge data according by the methodology proposed Mueller et al. (2013). These data were used to calculate several parameters, such as cross-sectional area and mean flow velocity, at each cross section. Using these parameters and density values, the Froude number (Fr_i), Reynolds number of the tributary "i" (Re_i), the momentum ratio (Mr) and discharge ratio (Q_r) were calculated from:

$$Fr_i = \frac{U_i}{\sqrt{g\,H_i}} \tag{1}$$

$$Re_i = \frac{U_i\,H_i}{\nu} \tag{2}$$

$$Mr = \frac{\rho_S Q_S U_S}{\rho_T Q_T U_T} \tag{3}$$

$$Q_r = \frac{Q_S}{Q_T} \tag{4}$$

where U_i (m s^{-1}) is the mean streamwise flow velocity "i", S is for the Saladillo River (considered the tributary in this study) and T is for the Tercero River (considered the main stream), H_i (m) is the mean depth of the tributary "i" (S or T), g (m s^{-2}) is acceleration due to gravity, ν (m^{2}s^{-1}) is the water kinematic viscosity, ρ is the water density (kg m^{-3}), and Q is the discharge (m^3 s^{-1}). Local vertical profiles of density in each tributary were computed using UNESCO's empirical method (Fofonoff and Millard, 1983) with data of water temperature and salinity (calculated using the conductivity and temperature data) collected by the YSI/Castaway CTD. Local vertical profiles of water temperature and electrical conductivity, corrected for temperature at 25 °C (due to the fact that conductivity varies with temperature and it is thus necessary express the conductivity at same temperature to enable comparison), were measured at ten different locations on each tributary and within the mixing zone (Fig. 2).

At each cross section, the mean flow velocity fields were characterized using VMT (Velocity Mapping Toolbox; Parsons et al., 2013). VMT is a computational program developed in Matlab® for processing and visualization of data acquired along multiple transects in rivers or other water bodies (Parsons et al., 2013). Maps of channel bathymetry were prepared using a continuous recording of depth values using the 1 MHz vertical beam of the ADCP, along a zig-zag trajectory, including upstream and downstream areas of the confluence (Fig. 2). These depth values were then interpolated on a grid covering the area of interest, using a kriging procedure at an average grid cell size of 3.2 × 3.7 m.

The water surface slopes of the Tercero and Saladillo rivers, as well as the downstream Carcarañá River (Fig. 5), were calculated from water surface elevation values recorded along the centerline of the rivers using a differential global positioning system (DGPS) recording at a frequency of 1 Hz. The DGPS was referenced to a base station (RTK system) located on the bank, allowing accuracies in the horizontal and vertical directions of ±10 mm and ±20 mm, respectively.

To visualize the patterns of surface flow, Spot 6 and 7 (©CNES 2017, Distribution Spot Image S.A.) and Ikonos images were used. The SPOT pictures were provided by the Argentina National Space Activities Comition (CONAE) and distributed by SPOT Image S.A. Spot 6 and 7 images have a spatial resolution of 6 m and 1.5 m on multispectral and panchromatic modes, respectively. Ikonos images (obtained from Google Earth®) have a 4 m resolution in multispectral mode. The images were projected in UTM zone 20S with WGS84 and linear filtering techniques in order to show the confluence flow patterns.

In addition to the principal survey period reported herein (08/13/2013), when ADCP and CTD data were collected throughout the junction, fieldwork on three other dates (06/07/2016, 03/08/2016 and 11/08/2016) collected flow discharge and CTD data in each tributary. These data were used to calculate density differences and momentum ratio, and these data aided interpretation of the flow mixing revealed by satellite images taken on 06/17/2016, 03/12/2016 and 11/04/2016.

4. Results

4.1. Main characteristics of the tributary flows

Table 1 shows the hydraulic parameters for the hydrological conditions studied herein (fieldwork 08/13/2013), where at this momentum ratio ($Mr = \rho_S Q_S U_S / \rho_T Q_T U_T = 0.25$), the shear layer intersected the outer bank of the bend a few meters downstream of the confluence (84 m from the stagnation point to the shear layer intersection with the outer bank, see Fig. 2). This indicates that the Saladillo River enters the confluence underneath the Tercero River, thus forming a density current.

The water surface slope of the Tercero River, herein taken as the main stream for the analyzed condition, was 0.18‰ and remained constant downstream of the confluence. A backwater effect was observed on the lower momentum tributary (Saladillo River) for the analyzed flow conditions. Profiles of electrical conductivity and temperature were evaluated to quantify the density differences for these flow conditions. Water temperature and electrical conductivity in the Tercero River inflow were 10.9 °C and 1.8 mS cm^{-1}, respectively, whereas water temperature and electrical conductivity values in the Saladillo River flow were 9.9 °C and 7.7 mS cm^{-1}, respectively (Fig. 4). The electrical conductivity values in Saladillo River are therefore more than four times greater than those in the Tercero River.

These values were then used to calculate the water density of each tributary (Fig. 4) that shows the Saladillo River has a higher density, but no vertical density gradients were present in either river.

4.2. Morphology of the confluence

The morphology of the confluence (Fig. 5) shows that the greatest depths are on the left bank of the Saladillo River upstream from the confluence (produced by human intervention consisting of an increase in depth of one portion of the cross section to improve the discharge capacity of the river section), which attains a maximum depth of 3.4 m. This zone of maximum depth also links into a zone of scour in the center of the junction, whose orientation approximately bisects the junction angle. A region of slightly higher elevation is present on the left bank immediately downstream of the downstream junction corner. Downstream of the confluence, the zone of maximum depth is located on

Table 1
Hydraulic parameters measured with ADCP.

Parameter	Unit	Tributary	Value
Flow discharge (Q)	[m^3 s^{-1}]	Tercero	19.9
		Saladillo	10.5
River width (W)	[m]	Tercero	40
		Saladillo	33
Cross section area (A)	[m^2]	Tercero	38
		Saladillo	42
Mean flow depth ($H = A / W$)	[m]	Tercero	0.9
		Saladillo	1.3
Mean velocity (U)	[m s^{-1}]	Tercero	0.52
		Saladillo	0.25
Reynolds number (Re_i)	Dimensionless	Tercero	4.7×10^5
		Saladillo	3.3×10^5
Froude number (Fr_i)	Dimensionless	Tercero	0.18
		Saladillo	0.07
Density (ρ)	kg m^{-3}	Tercero	1000.4
		Saladillo	1003.0
Momentum ratio (Mr)	Dimensionless		0.25

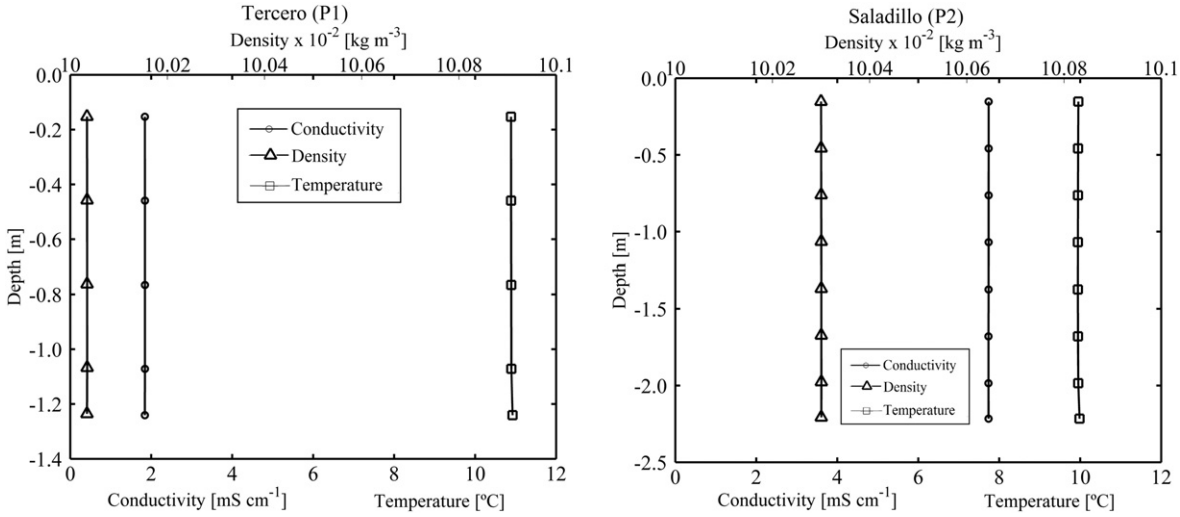

Fig. 4. Water conductivity, temperature and density profiles recorded on the incoming flows of the Tercero and Saladillo rivers (points P1 and P2, see Fig. 2 for locations).

the outer (right) bank, typical of flow in bends, and this region of maximum depth moves to the center of the channel.

Regarding the bed composition, the grain size distribution was determined by sieving and the hydrometer method (Díaz-Lozada, 2014) using the unified soil classification system (USCS). The results obtained for the Saladillo River and the Carcarañá River show a D_{50} of 0.1 mm, corresponding to silty sand.

4.3. Depth-averaged flow velocities

Depth-averaged flow velocities for eight cross sections in the confluence (Fig. 6) show that the core of maximum velocity is located near the inner bank of the bend (T, C1 and C2 sections). Maximum velocities are observed near the outer bank of the bend (C3 and C4 sections), thus showing typical bend flow hydrodynamics. In sections S and C1, low velocities are observed upstream of the shear layer, due to the existence of a stagnation zone at the upstream junction corner and the effect of backwater within the Saladillo River. The location of the shear layer is defined by the strong velocity gradient between the two flows, and marks the line at which the denser Saladillo River flow enters the confluence underneath the less dense Tercero River flow. Flow deflection is present where the flows join, as manifested downstream of the confluence by the change in direction of the velocity vectors of the converging flows. In cross sections C1 and C2, the velocity vectors have not yet

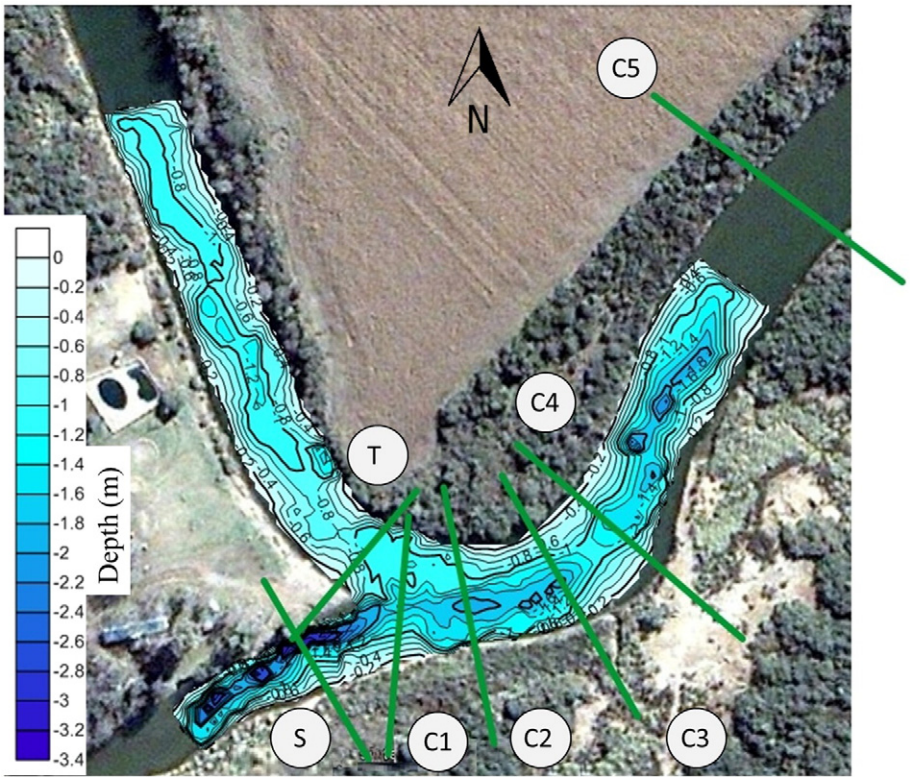

Fig. 5. Bathymetry of the confluence region.

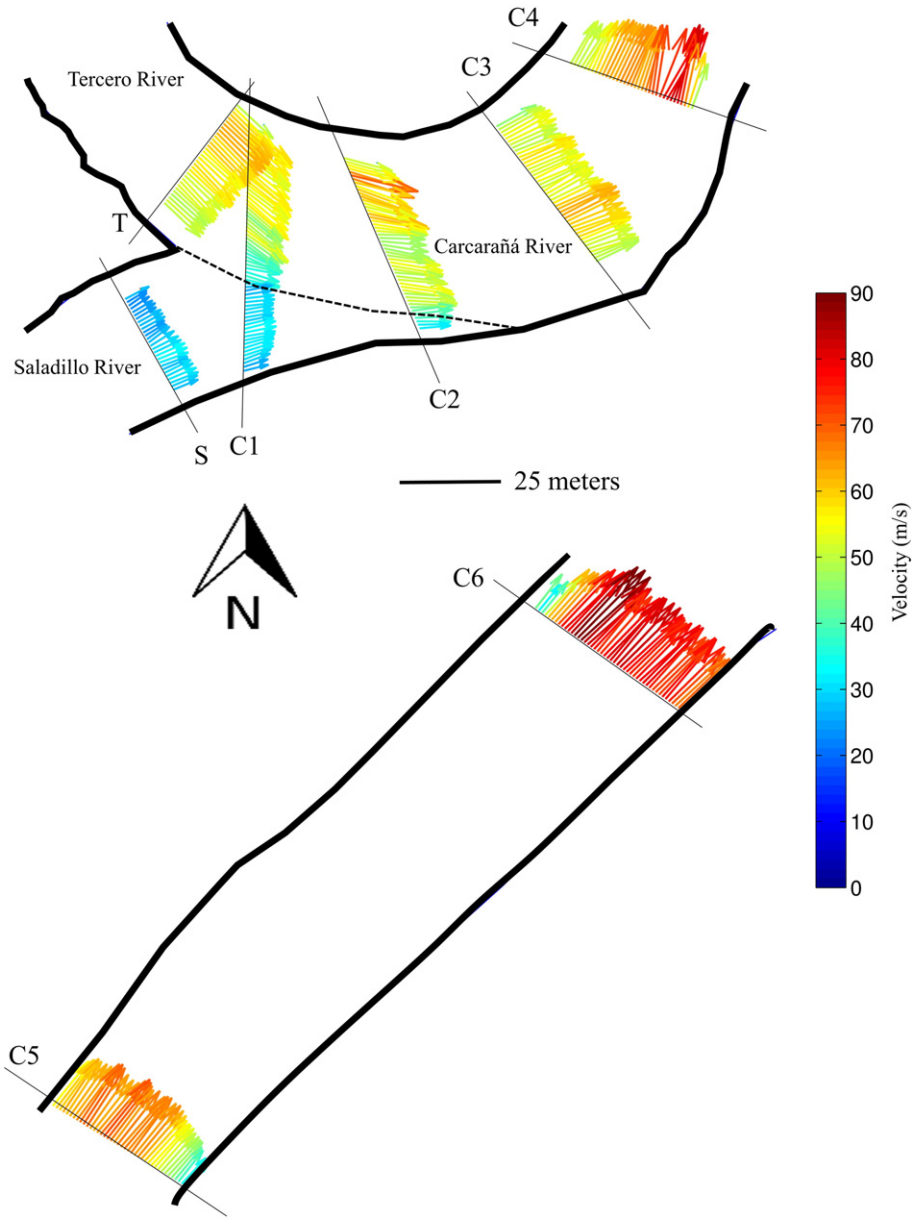

Fig. 6. Depth-averaged velocity vectors in the zone of the confluence of the Tercero and Saladillo rivers.

become completely aligned with the river direction, but at cross sections C3 and C4, they are completely aligned. These results provide no evidence of recirculation of flow, or flow separation, downstream of the lower junction corner, although the presence of a bar in this region may negate the production of flow separation (Best, 1988).

In order to examine the difference between near-bed and outer flow, we also present the depth-averaged flow vectors for two regions of flow (from the surface to a depth of 1.2 m and from the depth of 1.2 m deep to basal cell; Fig. 7) to investigate any differences in flow direction between these two regions. This plot shows that flow coming from the Saladillo River at cross section C1 moves across channel near the bed, moving across the region of scour. This flow pattern is a manifestation of the denser fluid from the tributary forming an underflow that moves across channel, in an area that may be expected to display helical flows at the junction center.

4.4. Analysis of cross-sectional flow field

The direction of flow in the confluence zone (Fig. 8) shows that at cross sections C1 and C2 the Saladillo River enters the confluence and flows underneath the Tercero River, and that the shear layer moves to the inner (left) bank at greater depths due to the density difference. This hydrodynamic pattern is also observed in cross section C3 (Fig. 8) where the shear layer near the water surface is closer to the outer bank of the bend.

The cross-sectional velocity fields clearly show that as the Tercero River enters the confluence, its flow is similar to that in a meander bend. At cross section T, the core of maximum velocities in the Tercero River is located on the inner (left) bank (Fig. 9T), with a typical flow pattern of secondary velocities (near-surface flow outward and near-bed flow inward), as calculated using the ZSD method (Zero Secondary Discharge; Parsons et al., 2013). Upstream of the confluence, the Saladillo River has low velocities (Fig. 9S). In section C1 (Fig. 9), the core of

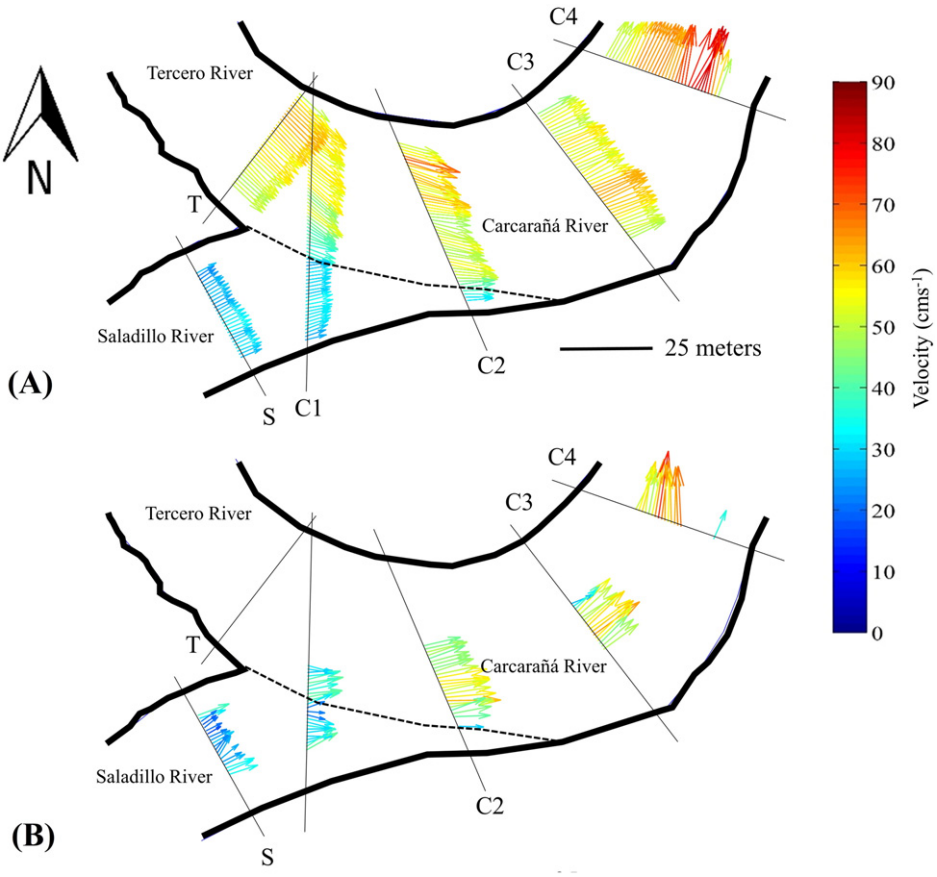

Fig. 7. Depth-averaged flow vectors for two regions of flow (A) from surface to 1.2 m and (B) 1.2 m – basal cell.

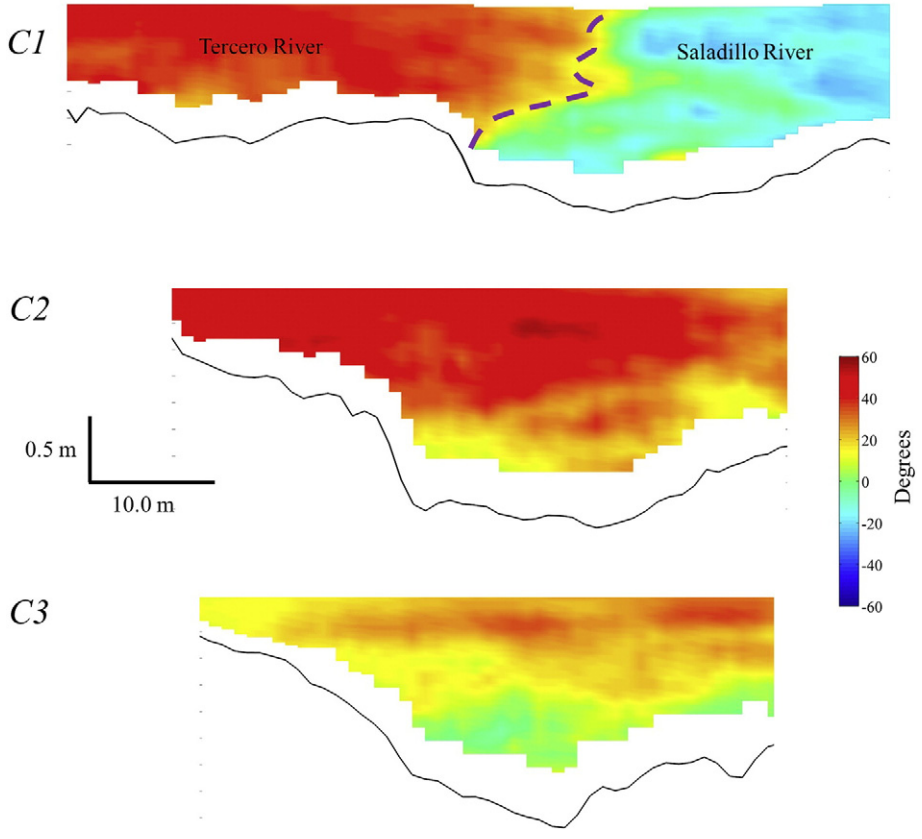

Fig. 8. Flow direction with respect to the principal mean flow in direction in each cross section.

maximum velocity is still located at the inner bank of the bend, but the secondary current vectors show that the Saladillo River flows underneath the Tercero River and produces an acceleration of secondary circulation in that zone. Furthermore, the intrusion of the Saladillo River intensifies the secondary currents generated by the flow within this curved channel. In cross section C2, the acceleration of the secondary current produced by the Saladillo River adds to the typical pattern of secondary flow present in bends. Downstream at cross section C3 (Fig. 9), the core of maximum velocity starts to move to the outer bank of the bend, and by cross section C4 this core is located at the outer bank. In cross section C4, a strong outward near-surface, and inward near-bed, flow can be observed. Secondary circulation has reversed from cross sections C4 to C5, and is not explained by the density differences but rather by the slight reversal in curvature through C4 to C6. Farther downstream, at cross section C6 that is located on a straight reach, the maximum velocities become located near the center of the cross section.

5. Discussion

5.1. Mixing processes downstream of the confluence

According to Fischer et al. (1979), the mixing length required to achieve a maximum deviation of 5% in the value of the concentration of a scalar (temperature, conductivity) can be given by:

$$L_m = 0.3\frac{UW^2}{\varepsilon_t} \tag{5}$$

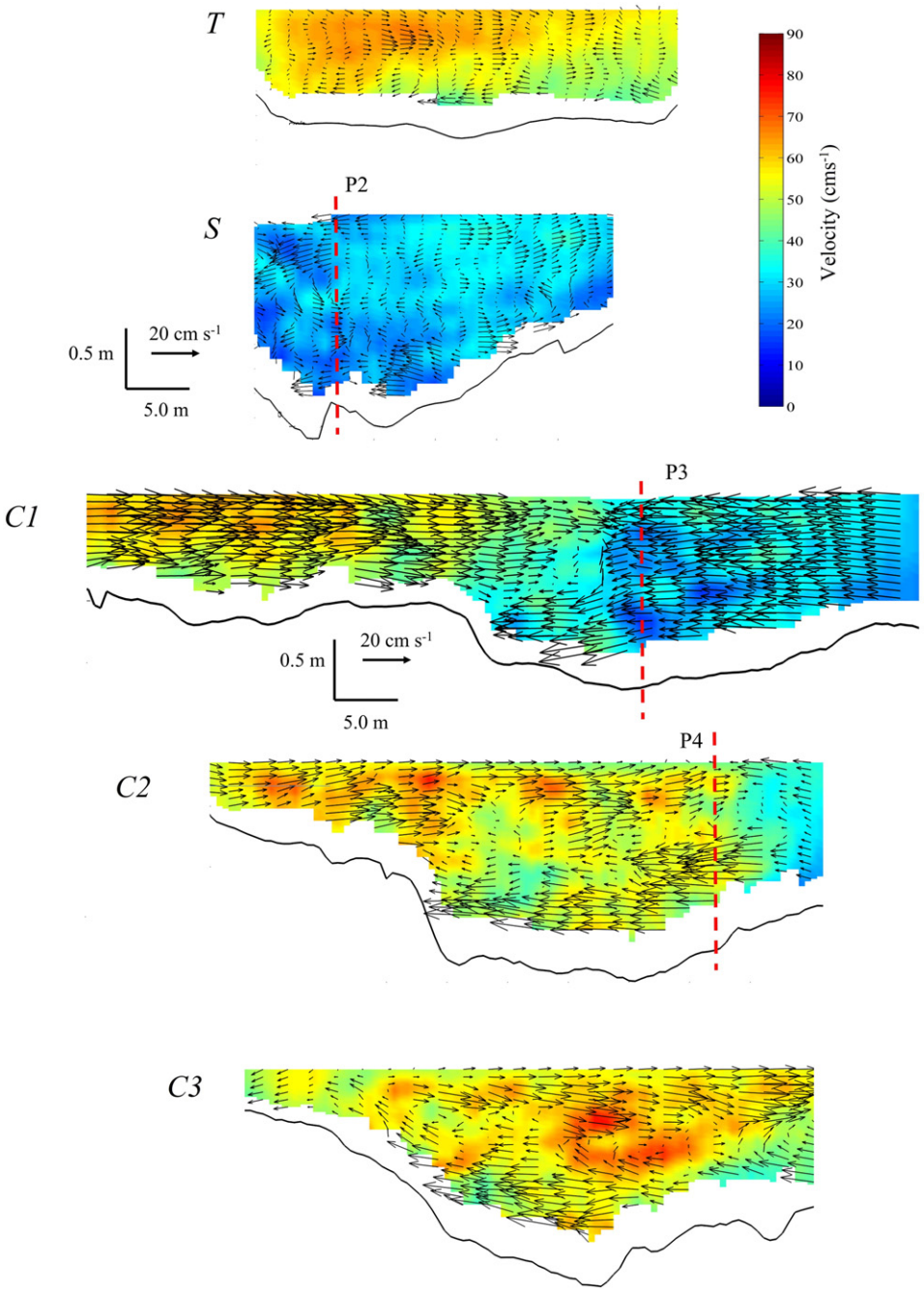

Fig. 9. Velocity magnitude in the cross sections, with the secondary current vectors calculated using the ZSD (Zero Stream Discharge) method.

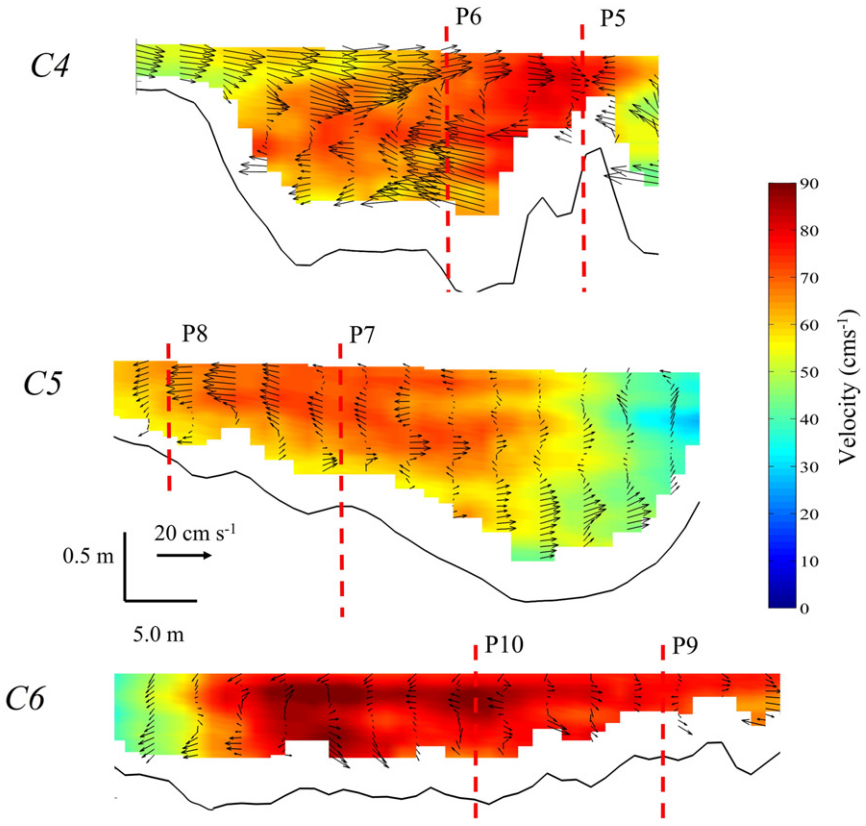

Fig. 9 (*continued*).

where U and W are the mean velocity and width of the river downstream of the confluence, respectively. The transverse mixing coefficient, ε_t is computed for a river bend according to Fischer et al. (1979) as:

$$\varepsilon_t = 25\frac{U^2H^2}{R^2u^*} \tag{6}$$

where H is the mean depth downstream of the confluence, R is the bend radius and u^* is the shear velocity that is computed as:

$$u^* = \sqrt{g \cdot H \cdot S_f} \tag{7}$$

where g is acceleration due to gravity and S_f is the energy (water surface) slope.

The values of all these parameters at the study site are summarized in Table 2, and have been used to estimate the complete transverse mixing length. The water surface slope was assumed equal to that measured downstream of the confluence.

Table 2
Hydraulic parameters measured downstream of the confluence and used to compute the theoretical mixing length.

Parameter	Unit	Value
R	[m]	65
U	[m/s]	0.55
H	[m]	1.1
W	[m]	49
S_f	[m/m]	0.00018
u^*	[m/s]	0.044
ε_t	[m^2/s]	0.055
L_m	[m]	7278

In order to evaluate the mixing length downstream of the confluence experimentally, water temperature and electrical conductivity profiles were recorded at different locations (Fig. 10). Profile P3 (located in the shear layer, see Fig. 2) shows that the three deeper points, located in cross section C1, have a conductivity value equal to the incoming flow of the Saladillo River (7.7 mS cm^{-1}) and this value decreases to 2.4 mS cm^{-1} at the water surface. A similar behavior is present at profile P4 close to the outer bank of bend and located in the shear layer, and this characteristic is due to the intrusion of higher density flow from the Saladillo River underneath the lower density flow from the Tercero River. Profiles P5 and P6 show that vertical mixing has been reached in P5, but not slightly farther across channel at P6 where it is still possible to see the intrusion of the Saladillo River.

Profiles P7 and P8, located in cross section C5, show that a complete vertical mixing has been reached due to the similarity of the conductivity values in each vertical profile, but the transverse mixing is not complete because there is a significant difference between the conductivity values registered in both profiles. Finally, in profiles P9 and P10 (cross section C6), the conductivity and temperature values are uniform in both the vertical and transverse directions, indicating that complete mixing has been achieved in the Carcarañá River approximately 450 m downstream of the apex of the confluence.

The estimated required length to achieve complete mixing using Eqs. (4), (5) and (6) is 7.28 km, and one order of magnitude larger than the observed length of 450 m. However, the relationships proposed by Fischer et al. (1979) assume (i) uniform flow and constant velocities in the entire domain, and (ii) complete mixing in the vertical direction and no density differences between the converging flows, which are not applicable at this channel junction.

Since the Saladillo River flows underneath water from the Tercero River, vertical mixing occurs first, with a characteristic time scale

much lower than the transverse mixing (with a river width of 40 m and mean depth of 0.9 m, Tz/Ty = 1975.3 $\varepsilon_t/\varepsilon_v$ where Tz and Ty are the times to achieve complete mixing in vertical and transverse direction, and ε_t and ε_v are the transverse and vertical dispersion coefficients). Such vertical mixing may be encouraged by the secondary flows present at the confluent meander bend.

To quantify the effects of density differences in estimating mixing downstream from a confluence, the buoyancy flux (B_f), defined as the

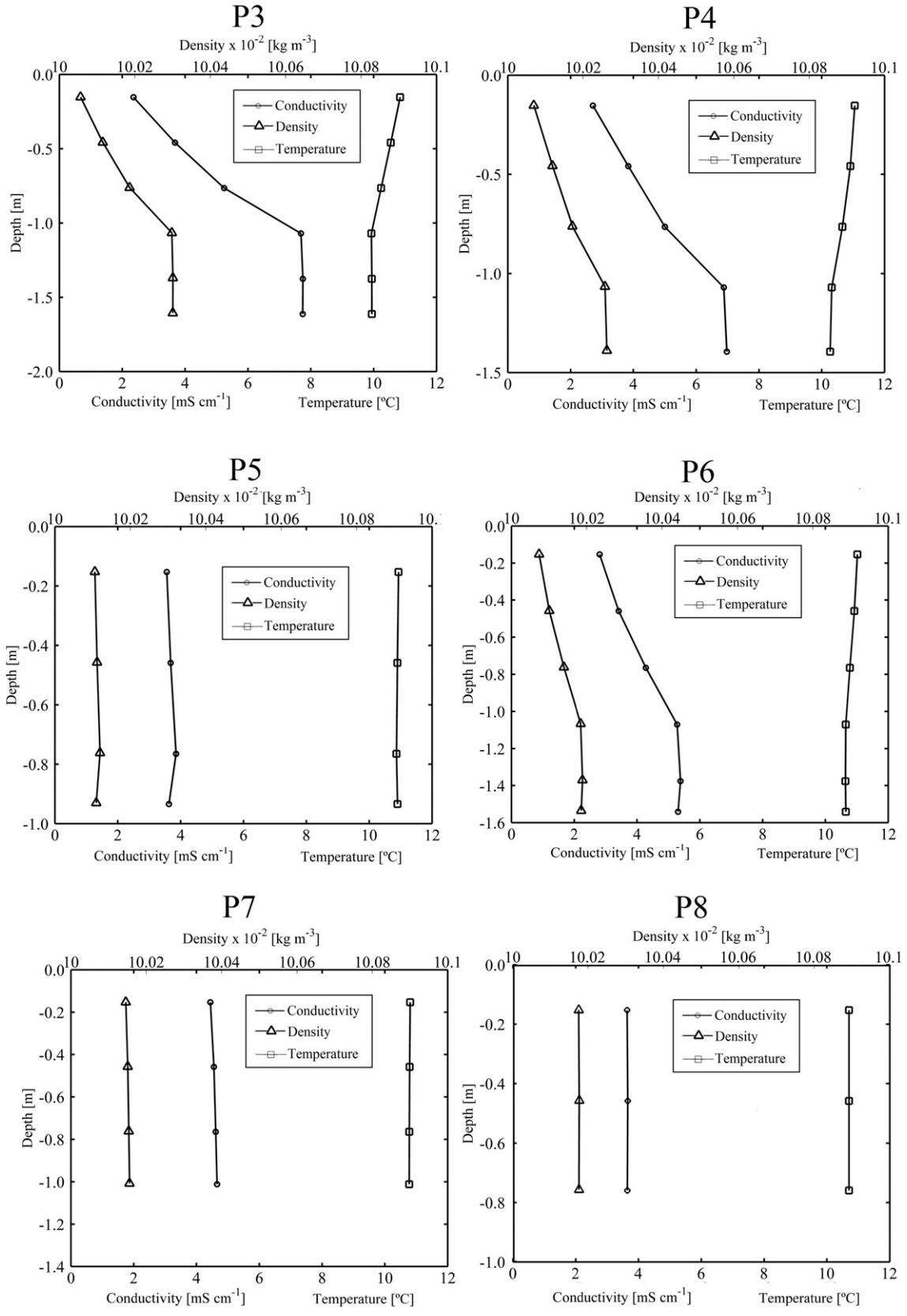

Fig. 10. Water electrical conductivity and temperature profiles recorded at different locations downstream of the confluence (see Fig. 2 for locations).

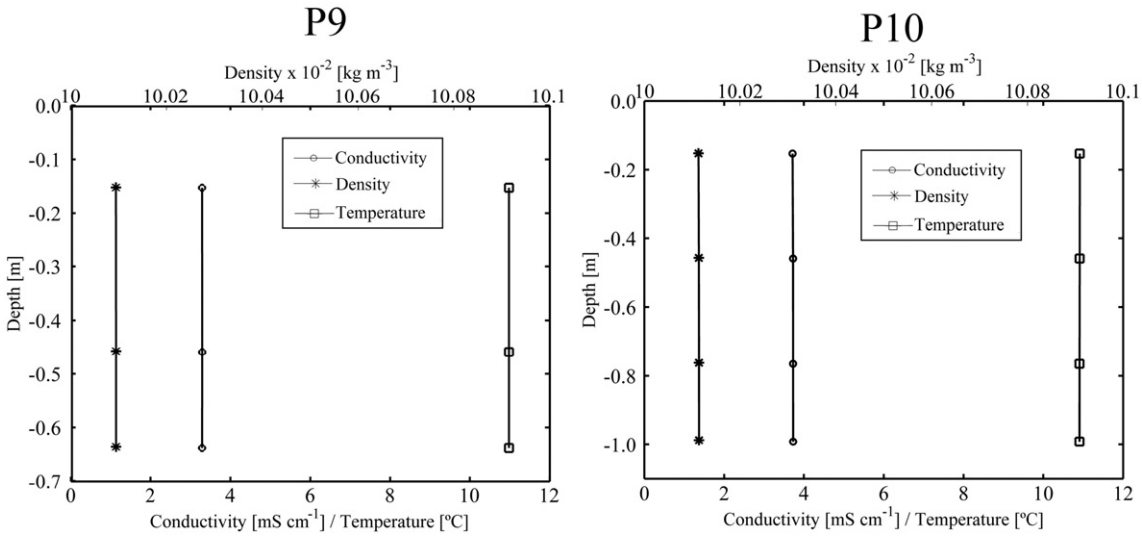

Fig. 10 (*continued*).

buoyant weight of fluid passing through a cross section per unit time reported by Fischer et al. (1979), can be used:

$$B_f = \frac{\Delta\rho}{\rho} \cdot g \cdot Q_e \tag{8}$$

where ρ is the receiving water body density (Tercero River herein), $\Delta\rho$ is the density difference between the tributaries and Q_e is the effluent discharge (Saladillo River herein). These parameters give rise to two dimensionless groups:

$$\frac{B_f}{H \cdot u^{*3}} \tag{9}$$

$$\frac{B_f}{W \cdot u^{*3}} \tag{10}$$

that summarize the relationship between the stabilizing influence of effluent per unit depth and width, respectively, and the available mixing capacity in the receiving water body. Results obtained in laboratory by Prych (1970) show that if $\frac{B_f}{H \cdot u^{*3}} < 5$, the effects of density differences are negligible in transverse mixing, and laboratory measurements by Schiller and Sayre (1973) indicate that if $\frac{B_f}{W \cdot u^{*3}} < 1$, vertical mixing is independent of density difference effects.

From the hydraulic parameters measured downstream of the confluence for the flow condition detailed herein at the Tercero - Saladillo river confluence (see Table 2), and a density difference between the tributaries of 2.61 kg m^{-3}, the values of these dimensionless groups are $\frac{B_f}{H \cdot u^{*3}} = 2866.80 > 5$, and $\frac{B_f}{W \cdot u^{*3}} = 64.35 > 1$. These values thus demonstrate that the effects of the density difference are not negligible, and could explain the observed rapid mixing between these tributaries.

Table 3
Discharge and density of each tributary of the confluence (for 06/07/2016, 03/08/2016 and 11/08/2016).

	Parameter	Unit	Tributary	Value
06/07/2016	Flow discharge (Q)	[m^3 s^{-1}]	Tercero	45.7
			Saladillo	68.2
	Density (ρ)	[kg m^{-3}]	Tercero	1000.6
			Saladillo	1003.2
03/08/2016	Flow discharge (Q)	[m^3 s^{-1}]	Tercero	122.4
			Saladillo	224.4
	Density (ρ)	[kg m^{-3}]	Tercero	997.8
			Saladillo	998.9
11/08/2016	Flow discharge (Q)	[m^3 s^{-1}]	Tercero	23.2
			Saladillo	119.4
	Density (ρ)	[kg m^{-3}]	Tercero	998.9
			Saladillo	1000.4

5.2. Confluence flow patterns at other hydrological conditions

Table 3 shows the flow discharge and density values measured in each tributary for three additional hydrological conditions (06/07/2016, 03/08/2016 and 11/08/2016). At all these times, the discharge of the Saladillo River was greater than the Tercero River ($Mr > 1$), opposite to the conditions characterized in detail above. On 06/07/2016, the density of the Saladillo River was important in yielding a momentum ratio a little greater than unity, and produced a shear layer that intersected the outer bank of the bend a few meters downstream of its entrance (140 m from the stagnation point to the shear layer intersection with the outer bank, see Fig. 11-A) on 08/13/2013. In the surveys of 03/08/2016 and 11/08/2016, the density of the Saladillo River is larger than the Tercero River, and the momentum ratio is significantly >1 that causes the shear layer to move toward the center of the confluence on 03/08/2016 (Fig. 11-B) or near to the inner bank of the bend on 11/08/2016 (Fig. 11-C).

Comparison between the conceptual model of confluent meander bend flow proposed by Roberts (2004; Fig. 1) and the hydrodynamic patterns observed herein (when the density differences are important, and the momentum ratio is <1) show several similarities and differences. In both cases, a stagnation zone exists near the apex of the confluence, but the model of Roberts (2004) indicates a region of flow separation downstream of the lower junction corner, a feature that was not observed herein. However, it should be noted that Roberts (2004) used sediment-free channels and that in the present study this region was characterized by a bar with higher elevation than the surrounding bed. In the unequal density confluent bend at the momentum ratio studied herein, the shear layer intersected the outer bank of the Saladillo River, and therefore the only way that the Saladillo River flow could enter the confluence was underneath the Tercero River. Due to flow of the Saladillo River underneath the Tercero River, a zone of eddies erupting on the flow surface was generated, which likely affected flow mixing at the confluence. In this zone, vertical mixing of the Saladillo River water produces an acceleration of the mixing process. Such mixing is not reported in the model of Roberts (2004) because this feature is generated by the difference density between tributary inflows. When the discharge of the Saladillo River is high and the

Fig. 11. Images of the Tercero (Ctalamochita) and Saladillo river confluence on: (A) 06/17/2016, with field measurements on 06/07/2016; (B) 03/12/2016, with field measurements on 03/08/2016, and (C) 11/04/2016, with field measurements on 11/08/2016.

momentum ratio is greater than unity, the confluence presents a behavior similar to that reported by Riley and Rhoads (2012).

The principal difference between the present results and those at the equi-density confluent meander bend reported by Riley and Rhoads (2012) is that in this previous study the shear layer lied in the center of the junction, shifted in position with changing momentum ratio, and did not intersect the bank edge. In a case where the shear layer intersects the bank for equal density tributaries, the tributary flow would be blocked, causing an even greater backwater effect until there was enough pressure gradient to force the shear layer away from the outer bank. In the present study, the density difference leads to plunging flow and a somewhat limited backwater effect. Thus, in the Tercero - Saladillo river confluence, when the momentum ratio is low (<1) the shear layer intersects the outer bank of the bend and, due to the density differences, the Saladillo River flows underneath the Tercero River. In comparison with the results of Lane et al. (2008) at the confluence of the Paraná and Paraguay rivers (where density differences are produced by the high sediment concentration of the Paraguay River), the mixing was more rapid when the discharge of the Paraguay River was high because in this condition the river has a greater sediment concentration and density, and thus forms an underflow beneath the Paraná River. When the discharge of the Saladillo River is low (a higher concentration of dissolved minerals and thus higher density difference), the hydrodynamic patterns are quite different and the mixing between the tributaries is faster in contrast with the results obtained by Lane et al. (2008) where the density difference occurs due to the high sediment concentration.

The results presented herein may hold important implications for the dispersal of sediment and morphodynamics of such sites. The ability of the dense underflow to create sediment transport across the post-confluent channel may provide a flow and sediment dynamics different to traditional models of junction flow (Best and Rhoads, 2008) either in the presence or absence of bed topography such as steps at the mouths of the tributary channels. Existing models of confluent flow often argue for the presence of helical, secondary flow cells, whether produced by water surface superelevation at the junction center, streamline curvature in the confluence or the effects of topography (e.g., Mosley, 1976; Best, 1988; Rhoads and Kenworthy, 1995; Rhoads, 1996; Best and Rhoads, 2008). Our data (Figs. 8 and 9) shows the movement of fluid, and thus potentially sediment in suspension and bedload transport, across channel. This may potentially negate, or modify, the presence of secondary 'helical' flow cells from this tributary and allow sediment transport, as bedload or suspended load, across the confluence and not segregated in pathways around the junction center as has been suggested in past work where density differences are absent (Best, 1988; Boyer et al., 2006). Indeed, at cross section C1 (Fig. 7), the basal flow can be seen to be moving across channel in the area of scour where previous work has suggested segregation of sediment from each tributary (Best, 1988; Boyer et al., 2006). These flow patterns may thus also have a significant influence on the mixing of nutrients and pollutants in regions where density underflows are present.

6. Conclusions

The confluent meander bend of the Tercero and Saladillo rivers generates different hydrodynamic patterns depending on the flow discharge and water density in each tributary. When the discharge of the Saladillo River is high, density differences are low and the momentum ratio is greater than unity, and the hydrodynamic processes in the confluence are similar to those reported by Riley and Rhoads (2012) for an equi-density confluent meander bend. However, when the discharge of the Saladillo River is low, or close to the mean flow discharge, the momentum ratio is low and density differences between the tributaries increase, due to a high dissolved salt concentration in the Saladillo River. This causes the hydrodynamics and mixing processes to differ substantially to those reported by Riley and Rhoads (2012), as the Saladillo River generates an underflow that spreads the more saline flow across channel. In this case, mixing between the two flows is more rapid despite the lower momentum ratio, thus illustrating the potential importance of density differences in determining the rate of mixing at such confluent meander bends. The mixing length observed at the Tercero-

Saladillo river confluence was one order of magnitude smaller than that estimated using the theoretical approach of Fischer et al. (1979), due to the lack of inclusion of density differences between the tributaries, and assumptions of uniform flow and full mixing in the vertical in the theoretical treatment. This highlights the need for more complete methodologies for predicting mixing rates and lengths at such sites of complex flow dynamics.

Acknowledgments

The authors thank Eliovac S.A. for providing the CTD used in the field work, and the thorough and stimulating reviews from the three referees and editor of Geomorphology.

References

Abrahams, A.D., 1984a. Channel networks: a geomorphological perspective. Water Resour. Res. 20 (2), 161–188.
Abrahams, A.D., 1984b. The development of tributaries of different sizes along winding streams and valleys. Water Resour. Res. 20 (12), 1791–1796.
Ashmore, P.E., Ferguson, R.I., Prestegaard, K.L., Ashworth, P.J., Paola, C., 1992. Secondary flow in anabranch confluences of a braided, gravel-bed stream. Earth Surf. Process. Landf. 17 (3), 299–311.
Best, J.L., 1986. The morphology of river channel confluences. Prog. Phys. Geogr. 10 (2), 157–174.
Best, J.L., 1987. Flow dynamics at river channel confluences: implications for sediment transport and bed morphology. In: Ethridge, F.G., Flores, R.M., Harvey, M.D. (Eds.), Recent Developments in Fluvial Sedimentology: Society of Economic Paleontologists and Mineralogists Special Publication No. 39. Society for Sedimentary Geology, Tulsa, OK, pp. 27–35.
Best, J.L., 1988. Sediment transport and bed morphology at river channel confluences. Sedimentology 35 (3), 481–498.
Best, J.L., Ashworth, P.J., 1997. Scour in large braided rivers and the recognition of sequence stratigraphic boundaries. Nature 387 (6630), 275–277.
Best, J.L., Reid, I., 1984. Separation zone at open channel junctions. J. Hydraul. Eng. 110 (11), 1588–1594.
Best, J.L., Rhoads, B.L., 2008. Sediment transport, bed morphology and the sedimentology of river channel confluences. In: Rice, S., Roy, A., Rhoads, B. (Eds.), River Confluences, Tributaries and the Fluvial Network. John Wiley & Sons, pp. 45–72.
Best, J.L., Roy, A.G., 1991. Mixing-layer distortion at the confluence of channels of different depth. Nature 350 (6317), 411–413.
Biron, P., De Serres, B., Best, J.L., 1993a. Shear layer turbulence at unequal depth channel confluence. In: Clifford, N.J., French, J.R., Hardisty, J. (Eds.), Turbulence: Perspectives on Flow and Sediment Transport, pp. 197–213.
Biron, P., Roy, A., Best, J.L., Boyer, C.J., 1993b. Bed morphology and sedimentology at the confluence of unequal depth channels. Geomorphology 8 (2), 115–129.
Biron, P., Best, J.L., Roy, A.G., 1996a. Effects of bed discordance on flow dynamics at open channel confluences. J. Hydraul. Eng. 122 (12), 676–682.
Biron, P., Roy, A.G., Best, J.L., 1996b. Turbulent flow structure at concordant and discordant open-channel confluences. Exp. Fluids 21, 437–446.
Bouchez, J.E., Lajeunesse, J., Gaillardet, C., France-Lanord, P., Dutra-Maia, L., Maurice, 2010. Turbulent mixing in the Amazon River: the isotopic memory of confluences. Earth Planet. Sci. Lett. 290, 37–43.
Boyer, C., Roy, A.G., Best, J.L., 2006. Dynamics of a river channel confluence with discordant beds: flow turbulence, bed load sediment transport, and bed morphology. J. Geophys. Res. Earth Surf. 111 (F4).
Bristow, C.S., Best, J.L., Roy, A.G., 1993. Morphology and facies models of channel confluences. Alluvial Sedimentation, pp. 91–100.
Callaway, C., 1902. On a cause of river curves. Geological Magazine (Decade IV). vol. 9, pp. 450–455.
Davis, W.M., 1903. The development of river meanders. The Geological Magazine, New Series, Decade IV. vol. 10, pp. 145–148.
De Serres, B., Roy, A.G., Biron, P.M., Best, J.L., 1999. Three-dimensional structure of flow at a confluence of river channels with discordant beds. Geomorphology 26 (4), 313–335.
Díaz-Lozada, J.M., 2014. Cuantificación y Caracterización del Escurrimiento Superficial de la Cuenca del Río Carcarañá. Master Science Thesis. FCEFYN-UNC, Córdoba, Argentina.
Díaz-Lozada, J.M., García, C.M., Herrero, H., Barchiesi, G.M., Romagnoli, M., Portapila, M., Brarda, J.P., 2015. Cuantificación del escurrimiento superficial de la cuenca del Río Carcarañá. Rev. Fac. Cien. Exact. Fisicas Nat. 2 (1), 59–72.
Fischer, H.B., 1969. The effects of bends on dispersion in streams. Water Resour. Res. 5, 496–506.
Fischer, H.B., List, E.J., Koh, R.C.Y., Imberger, J., Brooks, N.H., 1979. Mixing in Inland and Coastal Waters. Academic Press, Waltham.
Flint, J.J., 1980. Tributary arrangements in fluvial systems. Am. J. Sci. 280 (1), 26–45.
Fofonoff, N.P., Millard, R.C., 1983. Algorithms for computation of fundamental properties of seawater. UNESCO Technical Papers in Marine Science, Paris (53 p.).
Herrero, H.S., 2014. Evolución Espacial y Temporal de la Hidrodinámica en Confluencias Fluviales. PhD thesis. FCEFYN – UNC, Córdoba Argentina.
Herrero, H.S., García, C.M., Pedocchi, F., López, G., Szupiany, R.N., Pozzi-Piacenza, C.E., 2016. Flow structure at a confluence: experimental data and the bluff body analogy. J. Hydraul. Res. 54 (3), 263–274.
Hills, R., 1983. Tributary Confluences on Meandering Streams in MINNESOTA (Unpublished Survey).
Kenworthy, S.T., Rhoads, B.L., 1995. Hydrologic control of spatial patterns of suspended sediment concentration at a stream confluence. J. Hydrol. 168 (1), 251–263.
Lane, S.N., Parsons, D.R., Best, J.L., Orfeo, O., Kostaschuk, R.A., Hardy, R.J., 2008. Causes of rapid mixing at a junction of two large rivers: Rio Parana and Rio Paraguay, Argentina. J. Geophys. Res. Earth Surf. 113 (F2).
Laraque, A., Guyot, J.L., Filizola, N., 2009. Mixing processes in the Amazon River at the confluences of the Negro and Solimoes Rivers, Encontro das Aguas, Manaus, Brazil. Hydrol. Process. 23 (22), 3131.
Lewis, Q.W., Rhoads, B.L., 2015. Rates and patterns of thermal mixing at a small stream confluence under variable incoming flow conditions. Hydrol. Process. 29, 4442–4456.
Lyubimova, T., Lepikhin, A., Konovalov, V., Parshakova, Y., Tiunov, A., 2014. Formation of the density currents in the zone of confluence of two rivers. J. Hydrol. 508, 328–342.
Maurice-Bourgoin, L., Quemerais, B., Moreira-Turcq, P., Seyler, P., 2003. Transport, distribution and speciation of mercury in the Amazon River at the confluence of black and white waters of the Negro and Solimões Rivers. Hydrol. Process. 17, 1405–1417.
McLelland, S.J., Ashworth, P., Best, J.L., 1996. The origin and downstream development of coherent flow structures at channel junctions. In: Ashworth, P., Bennett, S.J., Best, J.L., McLelland, S.J. (Eds.), Coherent Flow Structures in Open Channels. John Wiley and Sons, Chichester, UK, pp. 459–490 (ISBN 9780471957232).
Moreira-Turcq, P.F., Seyler, P., Guyot, J.L., Etcheber, H., 2003. Characteristics of organic matter in the mixing zone of the Rio Negro and Rio Solimões of the Amazon River. Hydrol. Process. 17, 1393–1404.
Mosley, M.P., 1976. An experimental study of channel confluences. J. Geol. 84 (5), 535–562.
Mueller, D.S., Wagner, C.R., Rehmel, M.S., Oberg, K.A., Rainville, F., 2013. Measuring discharge with acoustic Doppler current profilers from a moving boat (ver. 2.0, December 2013). U.S. Geological Survey Techniques and Methods, Book 3 chap. A22. 0.3133/tm3A22 (95 p.).
Park, E., Latrubesse, E.M., 2015. Surface water types and sediment distribution patterns at the confluence of mega rivers: the Solimões-Amazon and Negro Rivers junction. Water Resour. Res. 51:6197–6213. https://doi.org/10.1002/2014WR016757.
Parsons, D.R., Best, J.L., Lane, S.N., Orfeo, O., Hardy, R.J., Kostaschuk, R., 2007. Form roughness and the absence of secondary flow in a large confluence–diffluence, Rio Paraná, Argentina. Earth Surf. Process. Landf. 32 (1), 155–162.
Parsons, D.R., Best, J.L., Lane, S.N., Kostaschuk, R.A., Hardy, R.J., Orfeo, O., Amsler, L.M., Szupiany, R.N., 2008. Large river channel confluences. River Confluences, Tributaries and the Fluvial Network, pp. 17–32.
Parsons, D.R., Jackson, P.R., Czuba, J.A., Engel, F.L., Rhoads, B.L., Oberg, K.A., Best, J.L., Mueller, D.S., Johnson, K.K., Riley, J.D., 2013. Velocity Mapping Toolbox (VMT): a processing and visualization suite for moving-vessel ADCP measurements. Earth Surf. Process. Landf. 38 (11), 1244–1260.
Prych, E.A., 1970. Effects of Density Differences on Lateral Mixing in Open-channel Flows. Report No. KH-R-21. W.M. Keck Engineering Laboratories - California Institute of Technology.
Ramón, C.L., Hoyer, A.B., Armengol, J., Dolz, J., Rueda, F.J., 2013. Mixing and circulation at the confluence of two rivers entering a meandering reservoir. Water Resour. Res. 49: 1429–1445. https://doi.org/10.1002/wrcr.20131.
Ramón, C., Armengol, J., Dolz, J., Prats, J., Rueda, F.J., 2014. Mixing dynamics at the confluence of two large rivers undergoing weak density variations. J. Geophys. Res. Oceans 119:2386–2402. https://doi.org/10.1002/2013JC009488.
Rhoads, B.L., 1996. Mean structure of transport-effective flows at an asymmetrical confluence when the main stream is dominant. Coherent Flow Structures in Open Channels, pp. 491–517.
Rhoads, B.L., Kenworthy, S.T., 1995. Flow structure at an asymmetrical stream confluence. Geomorphology 11 (4), 273–293.
Rhoads, B.L., Sukhodolov, A.N., 2001. Field investigation of three-dimensional flow structure at stream confluences: 1. Thermal mixing and time-averaged velocities. Water Resour. Res. 37 (9), 2393–2410.
Rhoads, B.L., Sukhodolov, A.N., 2004. Spatial and temporal structure of shear layer turbulence at a stream confluence. Water Resour. Res. 40 (6).
Rhoads, B.L., Riley, J.D., Mayer, D.R., 2009. Response of bed morphology and bed material texture to hydrological conditions at an asymmetrical stream confluence. Geomorphology 109 (3), 161–173.
Riley, J.D., Rhoads, B.L., 2012. Flow structure and channel morphology at a natural confluent meander bend. Geomorphology 163, 84–98.
Riley, J.D., Rhoads, B.L., Parsons, D.R., Johnson, K.K., 2014. Influence of junction angle on three-dimensional flow structure and bed morphology at confluent meander bends during different hydrological conditions. Earth Surf. Process. Landf. 40 (2), 252–271.
Roberts, M.V.T., 2004. Flow Dynamics at Open Channel Confluent-meander Bends. Ph.D. thesis. University of Leeds, Leeds, UK.
Roy, A.G., Bergeron, N., 1990. Flow and particle paths in a natural river confluence with coarse bed material. Geomorphology 3, 99–112.
Roy, A.G., Roy, R., Bergeron, N., 1988. Hydraulic geometry and changes in flow velocity at a river confluence with coarse bed material. Earth Surf. Process. Landf. 13, 583–598.
Rutherford, J.C., 1994. River Mixing. John Wiley & Son Ltd., New York (336 pp.).
Schiller, E.J., Sayre, W.W., 1973. Vertical Mixing of Heated Effluents in Open-channel Flow. Iowa Institute of Hydraulics Research (Rep. No. 148).
Sontek, Y.S.I., 2013. RiverSurveyor S5/M9 System Manual. San Diego.
Sukhodolov, A.N., Rhoads, B.L., 2001. Field investigation of three-dimensional flow structure at stream confluences: 2. Turbulence. Water Resour. Res. 37 (9), 2411–2424.

Szupiany, R.N., Amsler, M.L., Best, J.L., Parsons, D.R., 2007. Comparison of fixed-and moving-vessel flow measurements with an aDp in a large river. J. Hydraul. Eng. 133 (12), 1299–1309.
Szupiany, R.N., Amsler, M.L., Parsons, D.R., Best, J.L., 2009. Morphology, flow structure, and suspended bed sediment transport at two large braid-bar confluences. Water Resour. Res. 45 (5).
Trevethan, M., Martinelli, A., Oliveira, M., Ianniruberto, M., Gualtieri, C., 2015. Fluid mechanics, sediment transport and mixing about the confluence of Negro and Solimões rivers, Manaus, Brazil. E-Proceedings of the 36th IAHR World Congress, 28 June–3 July, 2015, Hague, The Netherlands (12 pp.).
Weigold, F., Baborowski, M., 2009. Consequences of delayed mixing for quality assessment of river water: example Mulde–Saale–Elbe. J. Hydrol. 369 (3), 296–304.
Yotsukura, N., Sayre, W.W., 1976. Transverse mixing in natural channels. Water Resour. Res. 12 (4), 695–704.